Deep-Sea Research I 66 (2012) 11–25

Contents lists available at SciVerse ScienceDirect

Deep-Sea Research I

journal homepage: www.elsevier.com/locate/dsri

# On the oceanic communication between the Western Subarctic Gyre and the deep Bering Sea

J. Clement Kinney *, W. Maslowski

*Naval Postgraduate School, Department of Oceanography, 833 Dyer Road, Monterey, CA 93943, USA*

ARTICLE INFO

*Article history:*
Received 27 October 2011
Received in revised form
15 March 2012
Accepted 1 April 2012
Available online 12 April 2012

*Keywords:*
Bering Sea
Alaskan Stream
Western Subarctic Gyre
Aleutian Island Passes
Near Strait
Kamchatka Strait

ABSTRACT

Sparse information is available on the communication between the northern North Pacific and the southern Bering Sea. We present results from a multi-decadal simulation of a high-resolution, pan-Arctic ice-ocean model to address the long-term mean and variability and synthesize limited observations in the Alaskan Stream, Western Subarctic Gyre, and southern Bering Sea. While the mean circulation in the Bering Sea basin is cyclonic, during the 26-year simulation meanders and eddies are continuously present throughout the region, which is consistent with observations from Cokelet and Stabeno (1997). Prediction (instead of prescription) of the Alaskan Stream and Aleutian throughflow allows reproduction of meanders and eddies in the Alaskan Stream and Kamchatka Current similar to those that have been observed previously (e.g. Crawford et al., 2000; Rogachev and Carmack, 2002; Rogachev and Gorin, 2004). Interannual variability in mass transport and property fluxes is particularly strong across the western Aleutian Island Passes, including Buldir Pass, Near Strait, and Kamchatka Strait. Much of this variability can be attributed to the presence of meanders and eddies found both north and south of the passes, which are found to directly cause periodic flow reversals and maxima in the western passes. Given that modeled flow reversals and maxima last for time periods ranging between three months and two years, short-term observations (months to few years) may not be representative of the actual mean flow. These extremes in the communication across the Aleutian Island Passes have a large impact on the oceanic environmental conditions in the southern Bering Sea and could directly impact biological species there and further downstream. Therefore, we identify a need for continuous monitoring of the flow through Buldir Pass, Near, and Kamchatka straits.

Published by Elsevier Ltd.

## 1. Introduction

The deep Bering Sea basin is bordered by the Aleutian Island Arc to the south, by the Bering Sea slope to the northeast, and by the Kamchatka Peninsula to the northwest. Depths greater than 3000 m are found throughout the basin, except in the vicinity of two large submarine features: Bowers Ridge (north of Amchitka Pass) and Shirshov Ridge, which extends southward from Kamchatka Peninsula.

The general circulation of the Bering Sea basin is typically described as cyclonic in the long-term mean. However, transport within the gyre can vary by more than 50% (Stabeno et al., 1999). Causes associated with this variation have been identified as either changes in the Alaskan Stream inflow (Overland et al., 1994) and/or variability of the wind-driven transport within the basin (Bond et al., 1994). The low-frequency variations in the wind stress curl account for approximately 1.5 Sv of the variability in the transport within the deep Bering Sea basin (Bond et al., 1994); however, the majority of the variability is due to variations in the curl on daily to monthly time scales.

High-resolution and large scale modeling of the Bering Sea basin and the Western Subarctic Gyre has been limited. Hermann et al. (2002) presented results from their regional, eddy-resolving model for 1995 and 1997. However, their limited domain (the southeast Bering Sea) did not include the Bering Sea basin. Instead, they focused on comparing hindcast results from 1995 and 1997, primarily of the eastern portion of the Bering Slope Current and the ANSC. Model results were also compared with Eulerian and Lagrangian observations.

Previous modeling work by Overland et al. (1994) focused on a limited domain: from 166°W to 157°E and from 46°N to the Bering shelf break. The primitive equation, three-layer hydrodynamic model had 1/8° resolution and excluded shallow regions $<500$ m deep. The Alaskan Stream was specified as a boundary condition at inflow and outflow points with a constant volume transport of 15 Sv. This approach allowed Overland et al. (1994) to realize general circulation features (e.g., complex cyclonic flow in the Bering Sea basin) similar to observations. However, they

* Corresponding author. Tel.: +1 831 656 3226; fax: +1 831 656 2712.
*E-mail address:* jlclemen@nps.edu (J. Clement Kinney).

0967-0637/$ - see front matter Published by Elsevier Ltd.
http://dx.doi.org/10.1016/j.dsr.2012.04.001

were not able to simulate the meanders in the Kamchatka Current that were identified by Stabeno and Reed (1994), nor were they able to show enough interannual variability in the flow through Near Strait to account for observations by Stabeno and Reed (1992) or Reed et al. (1993). The prescribed boundary condition for the Alaskan Stream and the climatological atmospheric forcing that was used may have prevented Overland et al. (1994) from simulating realistic variability in the flow through Near Strait. Although early observations (e.g., Reed 1984; Stabeno and Reed 1992) showed little eddy energy of the Alaskan Stream where it entered the Overland et al. (1994) domain (near 166°W), more recent observations are in stark contrast. For example, Crawford et al. (2000) observed 6 multi-year anticyclonic meanders and eddies in the Alaskan Stream using data from the TOPEX/Poseidon altimeter between 1992 and 1998. All of these mesoscale features formed east of 166°W, with some forming east of Kodiak Island.

More recent modeling work by Ezer and Oey (2010) focused on the relationship between the Alaskan Stream and the Bering Sea, with results showing that the strength of the Alaskan Stream imparts a nonlinear response in temperature and circulation in the Bering Sea. Wang et al. (2009) used a coupled sea ice-ocean model of the Bering Sea to examine seasonal variations in sea ice and ocean circulation, with results showing differing surface ocean circulation patterns on the shelf between summer and winter. Hu and Wang (2010) extended the model of Wang et al. (2009) to include tidal mixing and a wind-wave parameterization. They were able to show how tidal and wind-wave mixing are key factors in influencing the volume of the cold pool (water $<2$°C) on the Bering Sea shelf. Zhang et al. (2010) used a coupled sea ice-ocean model of the Bering Sea to determine the sea ice response to atmospheric and oceanic forcing. Results showed that the large interannual variability in ice cover was primarily controlled by the changes in wind-driven ice mass advection and the oceanic thermal front at the ice edge. Panteleev et al., 2011 used observations and model dynamics in the framework of a variational technique to obtain a mean dynamic topography for the Bering Sea. This work should be important for future studies, which use satellite observations to determine surface circulation in the region.

This article presents analyses of the general circulation within the Bering Sea basin and along the Aleutian Islands based on results from a high-resolution, pan-Arctic sea ice-ocean model. The long-term mean circulation and transport values from model results over the period 1979–2004 are depicted and discussed. In addition, time series of volume and property flux values across Aleutian Island Passes are shown and compared to available observations. Finally, the mesoscale meanders and eddies within the basin and along the Alaskan Stream are discussed and validated with limited observations.

## 2. Model description

The coupled sea ice-ocean model domain contains the sub-Arctic North Pacific (including the Sea of Japan and the Sea of Okhotsk) and North Atlantic Oceans, the Arctic Ocean, the Canadian Arctic Archipelago and the Nordic Seas (Fig. 1). This domain includes all oceanic areas of the northern hemisphere from 90°N to 55°N and most of the North Pacific down to 30°N. The region of interest for this paper, the northwestern North Pacific and the Bering Sea, is therefore far away from the artificially closed lateral boundaries, greatly reducing the potential effect of boundary conditions. Given the current limitations of supercomputing power and access, we have chosen to close the boundary at approximately 30°N in the Pacific in order to reduce the size of the domain and focus on high-resolution coverage of the Arctic Ocean and surrounding marginal seas. Model bathymetry is derived from two primary sources: ETOPO5 at 5 min resolution for the region south of 64°N and International Bathymetric Chart of the Arctic Ocean (Jakobsson et al., 2000) at 2.5 km resolution for the region north of 64°N.

The regional ocean model adapts the Los Alamos National Laboratory Parallel Ocean Program model (POP; Dukowicz and Smith, 1994). The POP model evolved from the Semtner and Chervin (1992) global ocean model with an added free surface (Killworth et al., 1991; Semtner, 1995). The free surface combined with high resolution allows the use of unsmoothed, very realistic bathymetry. This is important for representing steep bathymetry, such as the bathymetry around the Aleutian Islands, along the Aleutian Trench, and other continental slopes. The model uses Arakawa B grid as a finite differencing scheme (Mesinger and Arakawa 1976) and integrates the primitive equations in rotated spherical coordinates. Hydrostatic balance and the Bousinessq approximation are assumed in the model. The ocean model has 45 $z$-coordinate fixed vertical depth layers with eight levels in the upper 50 m and fifteen levels in the upper 200 m. The coupled sea ice–ocean model has a horizontal resolution of 1/12° (or approximately 9 km), which allows calculation of flow through the narrow straits of the Bering Sea and permits eddies with diameters as small as 36 km. However, recalling that the typical Rossby radius of deformation ranges between approximately 12–20 km in the Bering Sea (Chelton et al., 1998), the smallest eddies are not resolved (Maslowski et al., 2008b).

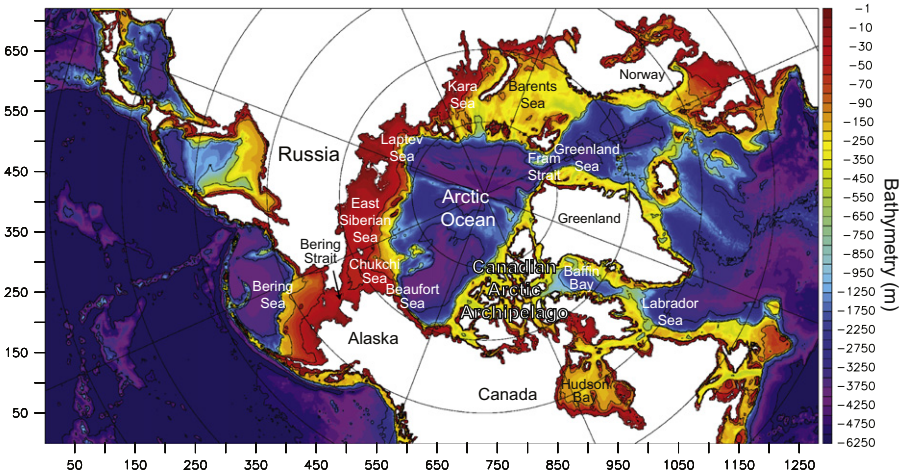


**Fig. 1.** 1/12° sea ice-ocean model domain and bathymetry (m).

The coefficients for vertical mixing are calculated as a function of Richardson number based on the Munk and Anderson (1948) approach with modifications adopted from Endoh et al. (1981) and Brooks (1994). The values of the biharmonic horizontal eddy viscosity ($B_M = -1.25 \times 10^{18}$ cm$^4$ s$^{-1}$) and diffusivity ($B_D = -5 \times 10^{17}$ cm$^4$ s$^{-1}$) coefficients do not vary horizontally. A no-slip boundary condition is applied at the lateral walls; and at the bottom, flow is required to follow the slope of the bathymetry, with no fluxes allowed through the bottom.

Yukon (and other Arctic) river runoff is included in the model as a virtual freshwater flux at the river mouth using the observed daily-averaged annual cycle of each river's discharge. In the Gulf of Alaska the freshwater flux from runoff (Royer, 1981) is introduced by restoring the surface ocean level (of 5 m) to climatological (Polar Science Center Hydrographic Climatology; PHC; Steele et al., 2001) monthly mean temperature and salinity values over a monthly time scale (as a correction term to the explicitly calculated fluxes between the ocean and overlying atmosphere or sea ice). This approach was used in part due to the lack of realistic discharge observations for the many small and ungauged rivers, which empty into the Gulf of Alaska, as well as a lack of domain-wide and time-varying precipitation/evaporation data. In addition, a 4°-wide band of ocean points along the domain boundary is restored to average PHC temperature and salinity climatology on a ten-day time scale.

The ocean model was initialized with climatological, three-dimensional temperature and salinity fields (PHC) and integrated for 48 years in a spin-up mode. During the spin-up, daily averaged annual climatological atmospheric forcing derived from 1979 to 1993 reanalysis from the European Centre for Medium-Range Weather Forecasts (ECMWF) was used for 27 years. The spin-up was continued using repeated 1979 ECMWF annual cycle for six years and then 1979–1981 interannual fields for the last 15 years of spin-up. This approach allows establishment of realistic ocean circulation representative of the time period at the beginning of the actual interannual integration. At the same time, the spin-up procedure was designed to force the model into a quasi-equilibrium state that is minimally sensitive to the specific initial conditions. The ocean time step is 8 min and the ice model time step is 48 min. The ECMWF atmospheric forcing fields include: 10-m east-west and north-south ($u$ and $v$) wind velocity components, 2-m air temperature, 2-m dew point, surface pressure, and incoming surface longwave and shortwave radiation. The final run with realistic daily averaged ECMWF interannual forcing starts in 1979 and continues through 2004. Results from this integration (26 years) are used for the following analyses.

## 3. General circulation

The Alaskan Stream flows primarily westward just south of the Aleutian Island Arc (Fig. 2). Please see Fig. 3 for regional place names and bathymetry. The Alaskan Stream is a major current of the northern North Pacific, as indicated by the high values of total kinetic energy (TKE) in Fig. 2a. TKE is calculated as

$$TKE = \frac{(u^2 + v^2)}{2} \quad (1)$$

with $u$ and $v$ representing the $x$- and $y$-components of velocity. TKE is useful for determining the relative speed of a current. The Alaskan Stream has a significant effect on the flow and property flux through the Aleutian Passes and, therefore, on the Bering Sea. The mean modeled volume transport is between 34 and 44 Sv, with intensification occurring downstream (Maslowski et al., 2008a).

Communication between the Bering Sea and the North Pacific (primarily the Alaskan Stream) occurs through several passes along the Aleutian Islands. Inflow through the central and eastern passes contributes to the eastward-flowing Aleutian North Slope Current (ANSC; Stabeno et al., 1999; Stabeno et al., 2009; Fig. 2a), which is located north of the Aleutian Islands. The generally eastward flow of the ANSC begins to turn northwestward between 177 and 167°W, forming the Bering Slope Current (BSC). The BSC extends from the eastern Aleutian Islands along the shelf-break toward the coast of Russia. Long-term mean volume transport was estimated to be approximately 2–3.5 Sv (Clement Kinney et al., 2009), however the BSC is more a system of eddies, rather than a continuous current (Okkonen, 1993; Clement Kinney et al., 2009). A major portion of the BSC separates from the slope around 180°, and gradually turns southwestward. The shallower portion is bathymetrically steered along the Siberian coast within the 500 m isobath, forming the Kamchatka Current. West of Shirshov Ridge, these two merge and flow primarily southward into the North Pacific Ocean. These general circulation features compare favorably with available observations published by Stabeno and Reed (1994), Verkhunov and Tkachenko (1992), Reed and Stabeno (1993) and Cokelet et al. (1996).

A schematic circulation for the region is proposed in Fig. 2b. This schematic is similar to that of Springer et al. (1999), which was based on work by Favorite (1976). In addition, our schematic includes a larger region and more detail than that of Springer et al. (1999). The strongest currents of the schematic are the Alaskan Stream and the East Kamchatka Current. The regions that show frequent eddy activity are indicated by spirals in Fig. 2b.

## 4. Volume and property flux across the Aleutian Island Passes

According to Stabeno et al. (1999), volume transport into the Bering Sea is highly variable on time scales of weeks to years. Inflow from the North Pacific into the Bering Sea occurs primarily through Near Strait, Buldir Pass, Amchitka Pass, and Amukta Pass (Stabeno and Reed, 1994). Outflow from the Bering Sea into the North Pacific occurs largely through Kamchatka Pass (Stabeno and Reed, 1994). Table 1 shows the model results of 26-year-mean (1979–2004) volume, heat, freshwater, and salt flux across each pass or strait shown in Fig. 3. Heat flux is referenced to the freezing temperature (based on salinity) and freshwater flux is referenced to 33.8 psu. Heat flux was calculated as the vertical and horizontal integral of: the heat (heat capacity multiplied by the difference between the temperature and the reference temperature) multiplied by velocity normal to the cross-section. Some passes were labeled alphabetically because they either did not have a recognized geographic place name or were artifacts of the 9 km grid cell spacing. The smallest islands were not resolved by the model bathymetry and at times created very shallow passes that are not present in reality. These alphabetically-labeled artificial passes had very low mean volume transport values, with most $< \pm 0.006$ Sv (the value at Strait C is $-0.136$ Sv). Model results have previously been compared with observations in Amukta Pass and Amchitka Pass (Maslowski et al. (2004); Maslowski et al., in prep.). Therefore, this current work will focus on the larger and deeper western passes including: Buldir Pass, Near Strait, and Kamchatka Strait.

### 4.1. Comparison of observed and modeled volume transports

Multi-year continuous observations of the flow through the western passes are not available. Available observations include data from satellite-tracked drifters (Stabeno and Reed, 1994) and

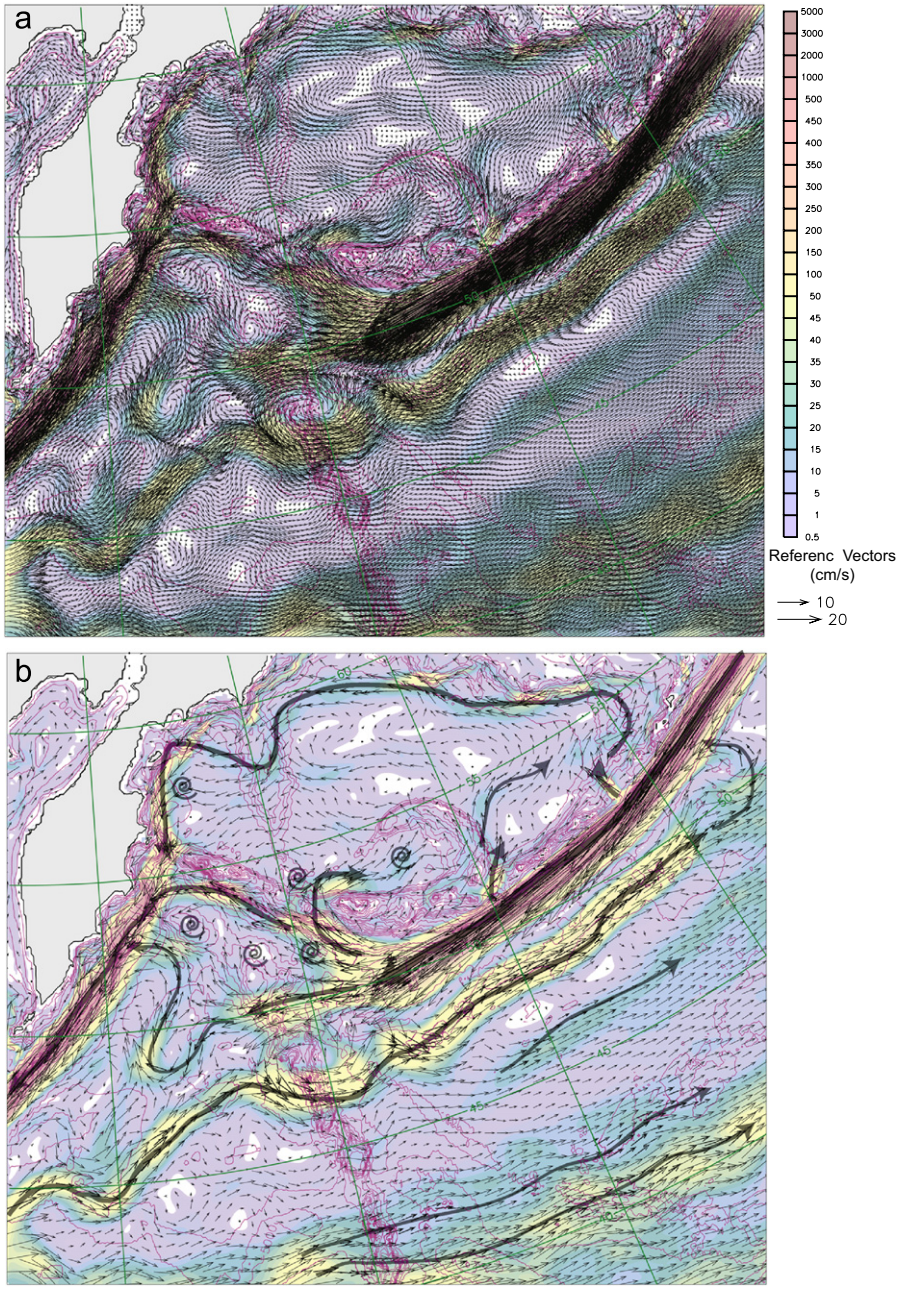


**Fig. 2.** (a) 26-year mean (1979–2004) upper 100 m circulation (vectors) and total kinetic energy (shading). Magenta contour lines represent bathymetry (m). Every second vector is shown. (b) Schematic circulation based on model results. Spirals indicate regions of frequent eddy activity.

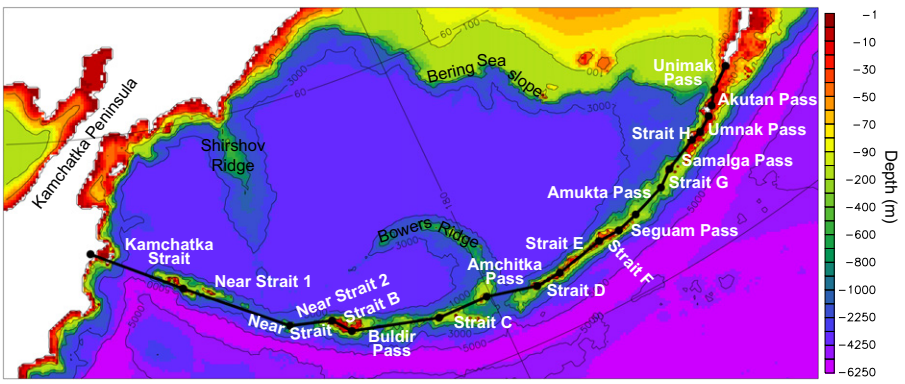


**Fig. 3.** Model bathymetry (m) of the deep Bering Sea. Black lines indicate the locations of cross-sections and white text indicates the names of these cross-sections.

short-term CTD measurements (e.g. Stabeno and Reed, 1992; Reed and Stabeno, 1993). Observations of the inflow through Buldir Pass were approximately 1 Sv during September 1992 (Stabeno and Reed, 1994), based on CTD measurements (see Table 2 for a comparison of modeled and observed volume transport values). The model results show a long-term mean of 1.2 Sv [standard deviation (S.D.)=1.566 Sv] net northward flow through Buldir Pass, averaged over 1979–2004.

Early observations of the northward flow through Near Strait range from 3.7 to 26 Sv (Arsen'ev, 1967; Ohtani, 1970; Hughes et al., 1974). Favorite (1974) concluded that a total of 10 Sv was a typical value. However, the methods behind all of these early observations cannot be considered precise. More recently, Reed and Stabeno, 1993 collected observations of volume flux through Near Strait during September 1992. Based on CTD casts, they found approximately 5 Sv of Alaskan Stream inflow through Near Strait. This compares well with the 26-year mean modeled net inflow of 5.057 Sv (a combination of the flow through sections labeled Near Strait 1 and Near Strait 2; S.D.=5.4 Sv; Table 1; Fig. 4). Based on satellite-tracked drifters released throughout the region, Stabeno and Reed (1992) noted an anomalous lack of inflow through Near Strait that began in summer 1990 and persisted at least through fall 1991. Modeled time series of volume flux through Near Strait over 26 years (Fig. 4) show seven time periods when the transport was near-zero or even reversed. These anomalies last from 3 months to almost 2 years. While the model results do not show a lack of inflow at exactly the same time period as Stabeno and Reed (1992), the processes underlying the anomaly appear to be the same. These processes will be discussed in the next section. Stabeno and Reed (1992) note that a strong and prolonged reduction of inflow into the Bering Sea would likely lead to a large cooling of subsurface waters. A reduction of inflow would also promote salinization of surface waters, thereby increasing the depth of wintertime convection. This prediction of a cooling of subsurface waters and salinization of surface waters is due to the fact that the inflow from the Alaskan Stream tends to be warmer and fresher than the Bering Sea water. The time series of volume transport through Near Strait appears to have a periodicity of approximately 3 years. This may be related to changes in the curl of the wind stress and/or the presence of planetary waves, which have been shown to be important within this region (Salmon, 1992).

Kamchatka Strait is the westernmost pass and is the primary location of southward flow out of the Bering Sea. Estimates of the Sverdrup transports within the deep Bering Sea basin imply that the local mean wind stress curl accounts for a significant portion (about 6 Sv) of the Kamchatka Current (Bond et al., 1994), which flows southward out of the Bering Sea via Kamchatka Strait. Outflow through Kamchatka Strait was estimated at approximately 11 Sv based on observations during April–May 1990 and at 6–7 Sv during October–November 1990 (Verkhunov and Tkachenko, 1992). Stabeno and Reed (1992) made observations in Kamchatka Strait that yielded an estimate of 6.8 Sv flowing southward during August 1991. However, they believe that this value is not typical of the Kamchatka flow, which instead is normally higher and closer to approximately 11 Sv. Panteleev et al. (2006) reconstructed the Bering Sea circulation as a variational inverse of the hydrographic and atmospheric climatologies, transport estimates through the Bering Strait, and surface drifter data. Based on this work, they estimate that the summer transport through Kamchatka Strait is 24 Sv southward, which is approximately twice as large as previous estimates. Panteleev et al. (2006) speculate that the difference between their estimate and previous observations is due to underestimation of the barotropic velocity component in the traditional transport estimates. The estimate of the baroclinic transport through Kamchatka Strait was approximately 10 Sv (Panteleev et al., 2006). The model was limited, however, by a domain that did not extend south of 55°N, which excluded Near Strait and other passes to the east. The NAME model results during 1979–2004 give a value of 8.9 Sv (S.D.=4.8 Sv) net southward flow, which is within the range of the observations (Table 2), though much lower than the estimate by Panteleev et al. (2006). A more detailed comparison would be required to resolve this discrepancy, including the effect of only summertime observational results throughout the Bering Sea and representation of eddies and flow reversals as well as exchanges through other passes in the estimates by Panteleev et al. (2006).

It is important to note that flow through these passes and straits is highly variable and controlled by mesoscale eddies (as discussed below) on time scales from weeks to years. Stabeno and Reed (1992) found a dramatic decrease in the inflow of Alaskan Stream water into the Bering Sea from summer 1990 to fall 1991. At the time of their publication, this was completely unexpected, since all previously available measurements showed relatively constant values of inflow and outflow. A high degree of variation occurs in the modeled time series of volume flux through the western passes and straits. Several strong flow reversals occur over the course of the 26-year time series in Near Strait and Buldir Pass. Five flow reversals occur in Kamchatka Strait, up to 3.9 Sv northward, during the 26-year simulation. The monthly mean volume flux time series through Near Strait and Kamchatka Strait are significantly correlated (at the 99% significance level). The correlation coefficient is −0.80 for the monthly mean values (Table 3). The correlation essentially means that when the inflow into the Bering Sea via Near Strait is strong, the outflow via Kamchatka Strait also tends to be strong. Also, when the flow through one of these straits is weak, the other would be expected to be weak. This correlation from model results is in qualitative agreement with observations by Stabeno and Reed (1992), which showed a weakened Near Strait inflow (approximately 3 Sv) coincident with a weakened Kamchatka Strait outflow (6–7 Sv) in August 1991. The volume transport through Kamchatka Strait is also significantly negatively correlated with the other passes located east of Near Strait, except for Amchitka Pass, which shows no correlation (Table 3). However, the correlations between Kamchatka Strait and the passes east of Near Strait are much lower in magnitude (−0.15 to −0.27) and, therefore, less important than the correlation between Kamchatka Strait and Near Strait.

Table 3, which includes correlation coefficients between all Aleutian Island Passes, also shows that volume transport through the easternmost passes (Unimak, Akutan, Samalga, Amukta, and Segaum) are all significantly correlated, except there is a lack of correlation between Amukta and Seguam. There is also a weak, but significant, correlation between Amchitka Pass and Buldir Pass. Significant negative correlations exist between Amchita Pass and Near Strait, as well as Buldir Pass and Near Strait.

### 4.2. Modeled heat fluxes

Twenty-six-year mean modeled heat fluxes across the Aleutian Island Passes are shown in Table 1. The reference temperature used to calculate the heat flux is the freezing temperature, which is based on salinity in this calculation. The highest net northward heat fluxes into the Bering Sea in descending order occur through Near Strait, Amchitka Pass, Amukta Pass and Buldir Pass (Fig. 5). The net monthly mean heat flux through Near Strait ranges from 203 TW southward to 483 TW northward. The range of variability is approximately 5.0 times the mean net heat flux (137 TW) at Near Strait. The net monthly mean heat flux through Amchitka Pass ranges from 96 TW southward to 287 TW northward. The range of variability is approximately 6.5 times the mean net heat

**Table 1**
26-year-mean fluxes across Aleutian Island cross-sections. Net volume flux (Net vol.) is given in Sv, with the standard deviation shown below each value of net volume flux. Positive (northward) volume flux (Pos. vol.) and negative (southward) volume flux (neg. vol.) values are also shown. The heat and freshwater flux values are shown in the same way. Heat flux values are given in TW, and freshwater flux values are given in mSv ($10^3$ $m^3$/s). Heat flux is referenced to the freezing temperature and freshwater flux is referenced to 33.8. The locations of the sections are shown in Fig. 3.

| Pass/strait | Net vol. /s.d. | Pos. vol. /Neg. vol. | Net heat /s.d. | Pos. heat/Neg. heat | Net FW/s.d. | Pos. FW/Neg. FW |
|---|---|---|---|---|---|---|
| Unimak | 0.069 | 0.096 | 1.933 | 2.968 | 4.110 | 5.492 |
| | 0.078 | −0.026 | 2.406 | −1.035 | 4.570 | −1.381 |
| Akutan | −0.001 | 0.011 | −0.209 | 0.305 | −0.013 | 0.589 |
| | 0.025 | −0.012 | 0.890 | −0.514 | 1.368 | −0.601 |
| Umnak | 0.003 | 0.015 | −0.026 | 0.485 | 0.195 | 0.797 |
| | 0.024 | −0.012 | 0.856 | −0.510 | 1.296 | −0.603 |
| Strait H | 0.002 | 0.003 | 0.058 | 0.124 | 0.083 | 0.161 |
| | 0.003 | −0.002 | 0.112 | −0.065 | 0.156 | −0.078 |
| Samalga | 0.041 | 0.344 | 1.085 | 10.760 | 2.355 | 15.145 |
| | 0.090 | −0.303 | 3.013 | −9.674 | 4.653 | −12.790 |
| Strait G | 0.040 | 0.116 | 1.131 | 3.721 | 2.111 | 6.067 |
| | 0.100 | −0.077 | 3.156 | −2.590 | 5.256 | −3.956 |
| Amukta | 1.601 | 1.753 | 50.378 | 55.408 | 64.783 | 71.284 |
| | 0.842 | −0.152 | 25.783 | −5.030 | 31.020 | −6.501 |
| Seguam | 0.026 | 0.102 | 0.724 | 3.441 | 1.375 | 4.767 |
| | 0.059 | −0.076 | 2.171 | −2.717 | 2.975 | −3.392 |
| Strait F | 0.006 | 0.029 | 0.121 | 0.983 | 0.306 | 1.315 |
| | 0.024 | −0.023 | 0.854 | −0.862 | 1.100 | −1.009 |
| Strait E | −0.004 | 0.058 | −0.426 | 1.944 | −0.002 | 2.659 |
| | 0.071 | −0.062 | 2.516 | −2.370 | 3.214 | −2.661 |
| Strait D | −0.006 | 0.046 | −0.367 | 1.579 | −0.196 | 2.117 |
| | 0.054 | −0.053 | 1.917 | −1.946 | 2.471 | −2.313 |
| Amchitka | 1.890 | 2.962 | 58.580 | 87.697 | 50.394 | 63.806 |
| | 2.299 | −1.072 | 64.668 | −29.117 | 32.053 | −13.412 |
| Strait C | −0.136 | 0.464 | −4.194 | 14.344 | −2.881 | 12.410 |
| | 0.757 | −0.600 | 23.156 | −18.537 | 18.225 | −15.291 |
| Buldir Pass | 1.216 | 2.178 | 36.673 | 66.280 | 22.635 | 45.088 |
| | 1.566 | −0.962 | 47.016 | −29.607 | 29.406 | −22.453 |
| Strait B | −0.003 | 0.009 | −0.081 | 0.302 | −0.092 | 0.332 |
| | 0.019 | −0.012 | 0.604 | −0.383 | 0.732 | −0.424 |
| Near Strait 1 | 2.520 | 3.806 | 70.282 | 106.062 | 22.686 | 39.576 |
| | 4.418 | −1.286 | 123.340 | −35.780 | 49.537 | −16.890 |
| Near Strait 2 | 2.537 | 9.283 | 66.455 | 238.023 | 15.180 | 70.384 |
| | 6.607 | −6.746 | 170.506 | −171.568 | 54.676 | −55.205 |
| Near Strait (total) | 5.057 | 13.089 | 136.737 | 344.085 | 37.866 | 109.961 |
| | 5.384 | −8.032 | 137.200 | −207.348 | 48.680 | −72.095 |
| Kamchatka | −8.903 | 2.983 | −195.267 | 59.597 | −116.494 | 13.729 |
| | 4.849 | −11.886 | 107.142 | −254.864 | 37.752 | −130.223 |

flux (59 TW) at Amchitka Pass. The net monthly mean heat flux through Amukta Pass ranges from 6 TW southward to 137 TW northward. The range of variability is approximately 2.9 times the mean net heat flux (50 TW) at Amukta Pass. The net monthly mean heat flux through Buldir Pass ranges from 74 TW southward to 142 TW northward. The range of variability is approximately

**Table 2**
Comparison of observed and modeled net volume transport values (Sv) for Buldir Pass, Near Strait, and Kamchatka Pass. Values for Buldir Pass and Near Strait are northward and values for Kamchatka Pass are southward. Model values are the mean of 26 years (1979–2004). Observed values are for time periods shown in parenthesis.

| Observation/model | Buldir Pass | Near Strait | Kamchatka Pass |
|---|---|---|---|
| NAME Model | 1.2 (net), 2.2 (northward), −1.0 (southward) | 5.1 (net), 13.1 (northward), −8.0 (southward) | −8.9 (net), 3.0 (northward), −11.9 (southward) |
| Stabeno and Reed (1993) | approximately 1 (Sept. 1992) | – | – |
| Favorite (1974) | – | 10 (1955–1974, discontinuous) | – |
| Reed and Stabeno (1993) | – | approximately 5 (Sept. 1992) | – |
| Stabeno and Reed (1992) | – | approximately 3 (Aug. 1991) | −6.8 (Aug. 1991) |
| Verkhunov and Tkachenko (1992) | – | – | approximately −11 (Oct.–Nov. 1990)<br>−6 to −7 (Apr–May 1990) |
| Panteleev et al. (2006) | – | – | −24 (1932–2004, discontinuous) |

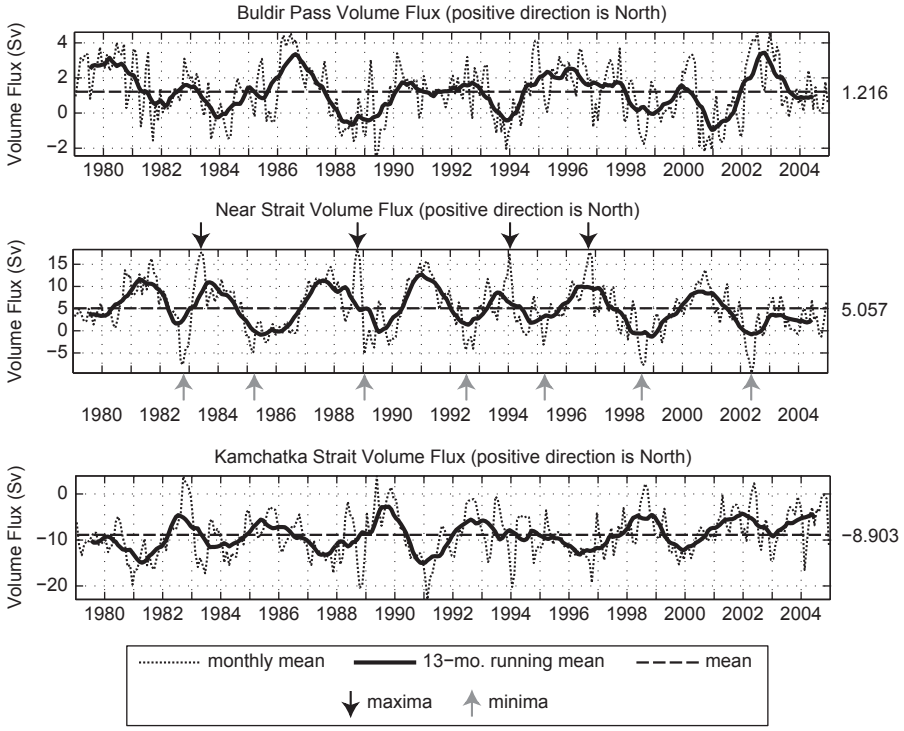


**Fig. 4.** Monthly mean time series of net volume transport (Sv; dotted line) through selected sections, as indicated. The black line represents a 13-month running mean and the dashed line indicates the overall mean. Means for each time series are shown to the right of each panel. Local maxima (black arrows) and minima/flow reversals (gray arrows) are indicated on the Near Strait time series. Maxima and minima are further discussed along with Figs. 11 and 12.

5.8 times the mean net heat flux (37 TW) at Buldir Pass. Southward heat flux occurs primarily through Kamchatka Strait with a southward mean of 255 TW and a northward mean of 60 TW, which gives a net mean heat flux of 195 TW southward. When the net mean heat flux is summed for all of the cross-sections shown in Table 1, the total net mean heat flux across the Aleutian Island Passes is 87 TW northward (S.D.=29 TW).

### 4.3. Modeled freshwater fluxes

Freshwater flux, using a reference salinity of 33.8, was calculated across the sections shown in Fig. 3. Almost 70% of the northward freshwater flux from the North Pacific into the Bering Sea occurs between Unimak and Amchitka Passes, even though only 37% of the volume transport inflow occurs there. The highest mean freshwater fluxes entering the Bering Sea occur through Amukta Pass, Amchitka Pass, Near Strait and Buldir Pass, in descending order (Fig. 6). The net monthly mean freshwater flux through Amukta Pass ranges from 3 mSv southward to 180 mSv northward. The range of variability is approximately 2.8 times the mean net heat flux (65 mSv) at Amukta Pass. The net monthly mean freshwater flux through Amchitka Pass ranges from 54 mSv southward to 135 mSv northward. The range of variability is approximately 3.8 times the mean net heat flux (50 mSv) at Amchitka Pass. The net monthly mean freshwater flux through Near Strait ranges from 110 mSv southward to 186 mSv northward. The range of variability is approximately 7.8 times the mean net heat flux (38 mSv) at Near Strait. The net monthly mean freshwater flux through Buldir Pass ranges from 48 mSv southward to 102 mSv northward. The range of variability is approximately 6.5 times the mean net heat flux (23 mSv) at Buldir Pass. When the net mean freshwater flux is summed for all of the cross-sections shown in Table 1, the total net mean freshwater flux across the Aleutian Island Passes is 67 mSv northward. (S.D.=51 mSv).

### 4.4. Annual cycles of fluxes

The annual cycles of volume, heat and freshwater transport are shown in Fig. 7 for the 5 passes with the largest transports among the Aleutian Island Passes. These include, Amukta, Amchitka, and

**Table 3**
Correlation coefficients and *p*-values (in parenthesis) among Aleutian Island passes and straits for monthly mean volume transport. Correlations that are significant at the 99% level are shown in bold.

| | Unimak | Akutan | Samalga | Amukta | Seguam | Amchitka | Buldir | Near | Kamchatka |
|---|---|---|---|---|---|---|---|---|---|
| Unimak | – | **0.93 (0.00)** | **0.81 (0.00)** | **0.34 (0.00)** | **0.47 (0.00)** | 0.04 (0.52) | 0.11 (0.04) | 0.01 (0.92) | **−0.21 (0.00)** |
| Akutan | – | – | **0.88 (0.00)** | **0.33 (0.00)** | **0.57 (0.00)** | 0.02 (0.77) | 0.12 (0.03) | 0.06 (0.33) | **−0.27 (0.00)** |
| Samalga | – | – | – | **0.22 (0.00)** | **0.62 (0.00)** | −0.02 (0.77) | 0.06 (0.28) | 0.05 (0.41) | **−0.21 (0.00)** |
| Amukta | – | – | – | – | 0.07 (0.25) | −0.03 (0.55) | −0.09 (0.12) | 0.05 (0.34) | **−0.23 (0.00)** |
| Segaum | – | – | – | – | – | −0.04 (0.44) | 0.07 (0.20) | 0.05 (0.41) | **−0.16 (0.01)** |
| Amchitka | – | – | – | – | – | – | **0.16 (0.00)** | **−0.48 (0.00)** | 0.00 (0.98) |
| Buldir | – | – | – | – | – | – | – | **−0.18 (0.00)** | **−0.15 (0.01)** |
| Near | – | – | – | – | – | – | – | – | **−0.80 (0.00)** |
| Kamchatka | – | – | – | – | – | – | . | – | – |

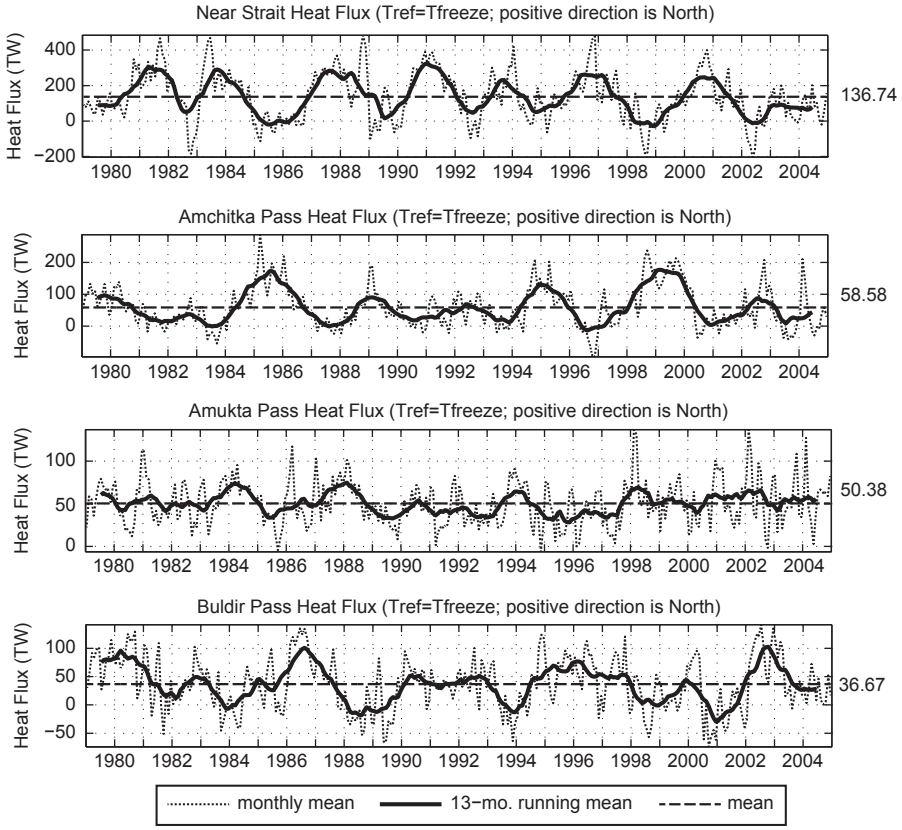


**Fig. 5.** Monthly mean (dotted line), 13-month running mean (black line) and overall mean (dashed line) heat flux through selected passes as labeled. Heat flux is referenced to the freezing temperature, which is based on salinity.

Buldir passes, as well as Near and Kamchatka straits. The annual cycles of volume, heat and freshwater transport have very similar shapes for the 3 easternmost passes (Amukta, Amchitka, and Buldir Passes) and at Kamchatka Strait. Freshwater transport differs slightly from volume and heat transport at Kamchatka Strait, in that it is less variable over the course of a year.

The annual cycle appears to play a significant role in the total flux of volume and properties within the eastern and central passes. For example, the annual cycle of volume transport ranges between approximately 0.75 and 2.25 Sv across Amukta Pass, which is approximately equal to the mean transport of 1.6 Sv. Similarly, at Amchitka Pass the annual cycle of volume transport ranges between approximately 1 and 3 Sv, which is, again, approximately equal to the overall mean transport of 1.9 Sv. The annual cycle at Buldir Pass is still important with a range of approximately 0.72–1.6 Sv, compared to an overall mean of 1.2 Sv. In addition, it appears that observations made during September 1992 by Stabeno and Reed (1994) were collected during the modeled minimum of the annual cycle. Model results show that the September mean transport is 0.72 Sv net northward (averaged over 1979–2004). Therefore, the observed value during September 1992 of approximately 1 Sv may be an underestimate of the long-term mean.

The annual cycle appears to be much less important at Near and Kamchatka straits. At Near Strait the volume transport annual cycle ranges from approximately 4.3 to 6 Sv, while the overall mean is 5.1 Sv. Similarly, at Kamchatka Strait the volume transport annual cycle ranges from −12 to −7.2 Sv with an overall mean of −8.9 Sv.

## 5. Mesoscale eddies in the Alaskan stream and the deep basin

### 5.1. Eddies in the deep Bering sea basin

The Bering Sea circulation over the deep basin is cyclonic in the mean, as shown in Fig. 2. However, animations of monthly

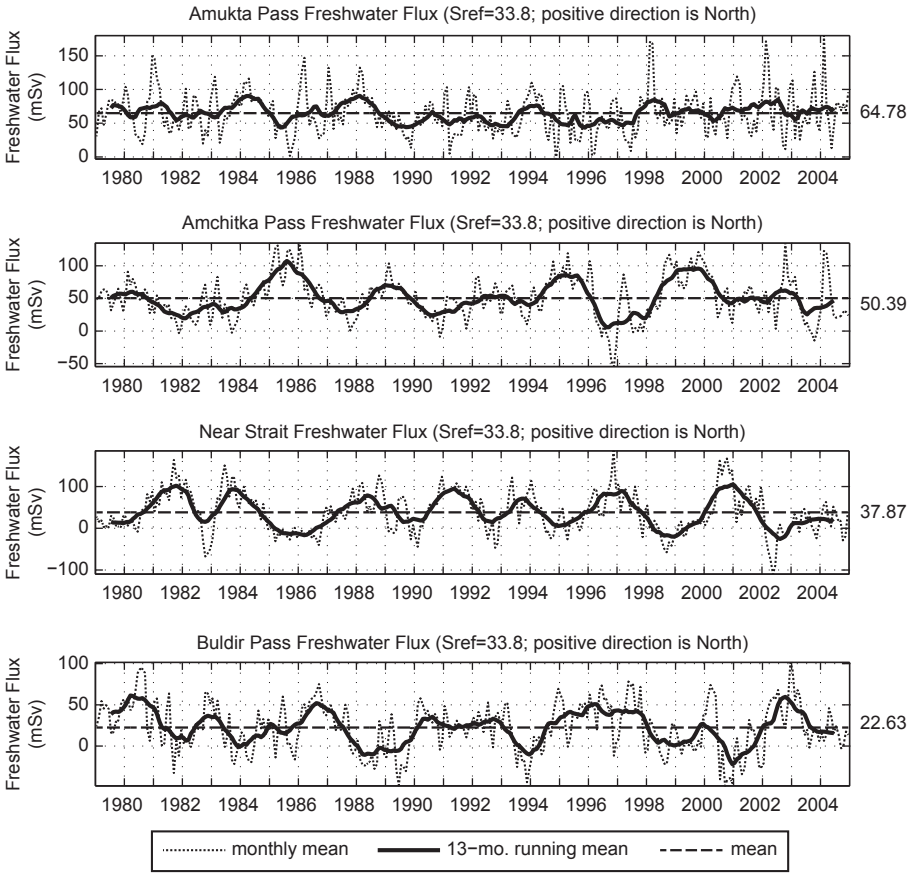


**Fig. 6.** Monthly mean (dotted line), 13-month running mean (black line) and overall mean (dashed line) freshwater flux through selected passes as labeled. Freshwater flux is referenced to 33.8 psu.

mean model results over the 26-year simulation show frequent and complex eddy activity throughout this area. For instance, at least 14 mesoscale eddies and meanders are present in the Bering Sea during June 1987 (Clement Kinney and Maslowski, 2008), as shown in Fig. 8. Half of these are anticyclonic and the other half are cyclonic. Diameters of these eddies are 120 km and greater and velocities are up to 40 cm/s. Lifetimes of these eddies are typically a few months. The 9 km horizontal resolution of the model makes it possible to resolve eddies with diameters as small as 36 km, however, the smallest eddies are likely not resolved, recalling that the Bering Sea has a Rossby radius of deformation of approximately 12–20 km according to Chelton et al. (1998).

Observations of eddies in the deep Bering Sea basin have been made by Cokelet et al. (1996) and Stabeno and Reed (1994), among others (e.g., Solomon and Ahlnäs, 1978; Kinder et al., 1980; Paluszkiewicz and Niebauer, 1984). Stabeno and Reed (1994) observed a large anticyclonic eddy west of Bowers Ridge that had a diameter of approximately 200 km and velocities of 30–40 cm/s, which is similar in size and velocity to those from the model. Cokelet et al. (1996) also observed a strong anticyclonic eddy there and suggested that it may be a recurring feature.

Schumacher and Stabeno (1994) suggest several possible mechanisms for the formation of eddies in this region, including instabilities, wind forcing, strong flows through the passes, and topographic interactions. Cokelet et al. (1996) suggest that instabilities along the Bering Slope and Kamchatka Current and interactions with canyons and embayments at the landward edge of these currents, as well as inflows through the Aleutian Island Passes, may be responsible for eddy generation. Stabeno and Reed (1994) observed several eddies and meanders within the Kamchatka Current and the Bering Sea Basin by utilizing satellite-tracked drifters. Several anticyclonic eddies were observed in the western side of the basin and resulted from the interaction of the Kamchatka Current with topographic features. Stabeno and Reed (1994) suspect that these features are semi-permanent, since they appeared in drifter trajectories from more than one year.

Model results during June 1987 (Fig. 8) show two anticyclonic eddies associated with the Kamchatka Current during June 1987 (KCA1 and KCA2 in Fig. 8). A cyclonic eddy (part of a counter-rotating pair) is also present near the Kamchatka Current at that time (labeled KCC in Fig. 8). The southernmost eddy (KCA1) originated along the western edge of Shirshov Ridge above the 300 m isobath in March 1987. It continued to strengthen and move southwestward until it dissipated in August 1987 approximately 70 km south of the position shown in Fig. 8. The northernmost anticyclonic eddy (KCA2) separated from KCA1 during May 1987 along the western edge of Shirshov Ridge. (Although the 4 cm sea surface height anomaly contour line (blue line in Fig. 8) does not enclose KCA2, the circulation is, in fact, closed) In contrast to KCA1, the position of KCA2 remained fixed until it dissipated in January 1988.

A vertical section of potential temperature through KCA1 in the Kamchatka Current (Fig. 9; cross-section location shown in Fig. 8) shows the cold core of the eddy with temperatures less than 1 °C from approximately 25–250 m depth. The anticyclone reversed the flow of this boundary current to over 15 cm/s northward, with a (local) southerly flow approximately 75 km further offshore due to the eddy. Temperatures were up to 2.5 °C colder than the 26-year mean within the core of the eddy. Typical June temperatures in this location are 1.5–3 °C and the usual speed of the southward-flowing Kamchatka Current is up to 9 cm/s in the core (Fig. 9). The colder water originates north of Shirshov

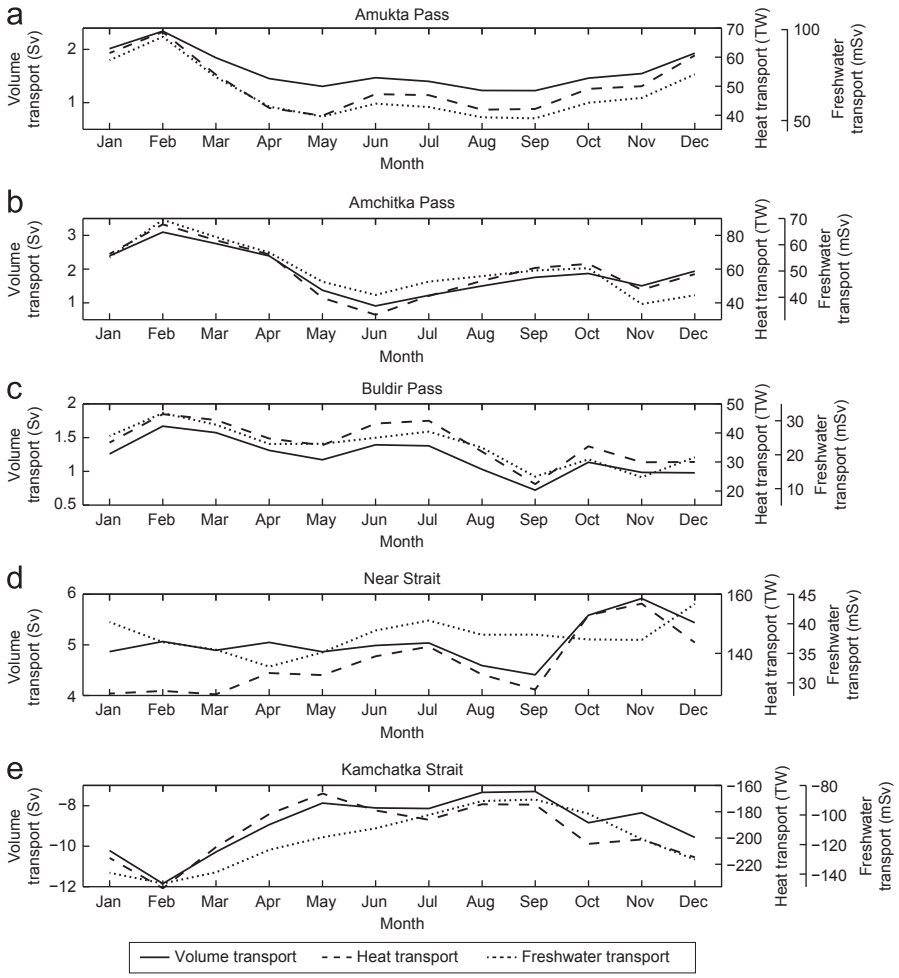


**Fig. 7.** Annual cycle of volume transport (Sv), heat transport (TW), and freshwater transport (mSv) through (a) Amukta Pass, (b) Amchita Pass, (c) Buldir Pass, (d) near Strait, and (e) Kamchatka Strait. Heat transport is referenced to the freezing temperature and freshwater transport is referenced to $S=33.8$.

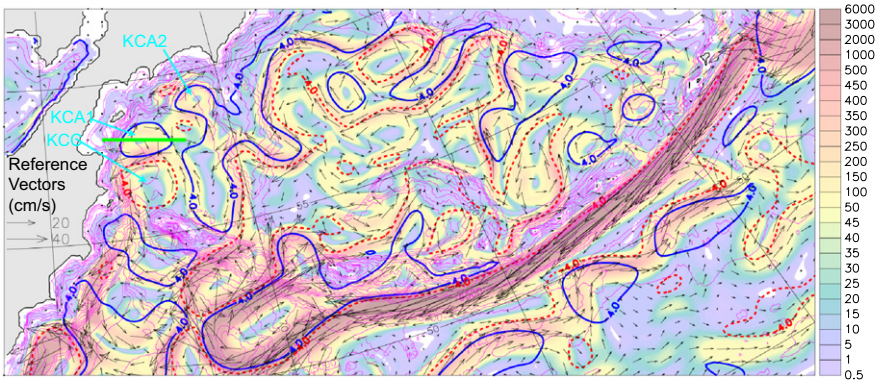


**Fig. 8.** June 1987 upper 100 m circulation (vectors) and total kinetic energy (shading). Sea surface height anomalies of +4 cm and −4 cm are represented by blue and red dashed contour lines, respectively. Magenta contour lines represent bathymetry (m). The green line indicates the position of a cross section shown in Fig. 9. Every sixth vector is shown (For interpretation of the references to color in this figure legend, the reader is referred to the web version of this article.).

Ridge and is carried southward by the Kamchatka Current. A shallower thermocline is also apparent when the eddy is present, as shown by the temperature difference Fig. 9c (negative values just below the surface). The temperature signature of the modeled eddy is similar to observations by Rogachev et al. (2007) of cold-core eddies within the Kamchatka Current. One of the observed eddies was located just south of Kamchatka Strait and displayed temperatures near 0 °C at its core.

The salinity section reveals a strong displacement of isohalines ($>200$ m) across KCA1 during June 1987, as compared to the 26-year mean (1979–2004; Fig. 10a). The relatively fresh core of the anticyclone exhibited salinities of 32.5 as deep as 200 m. Typically, water with such a fresh signal is confined to the shelf (Fig. 10b). Salinity differences (between June 1987 and the 26-year mean June) show that the core of the eddy was up to 0.75 psu fresher than average, as well as approximately 0.15 psu

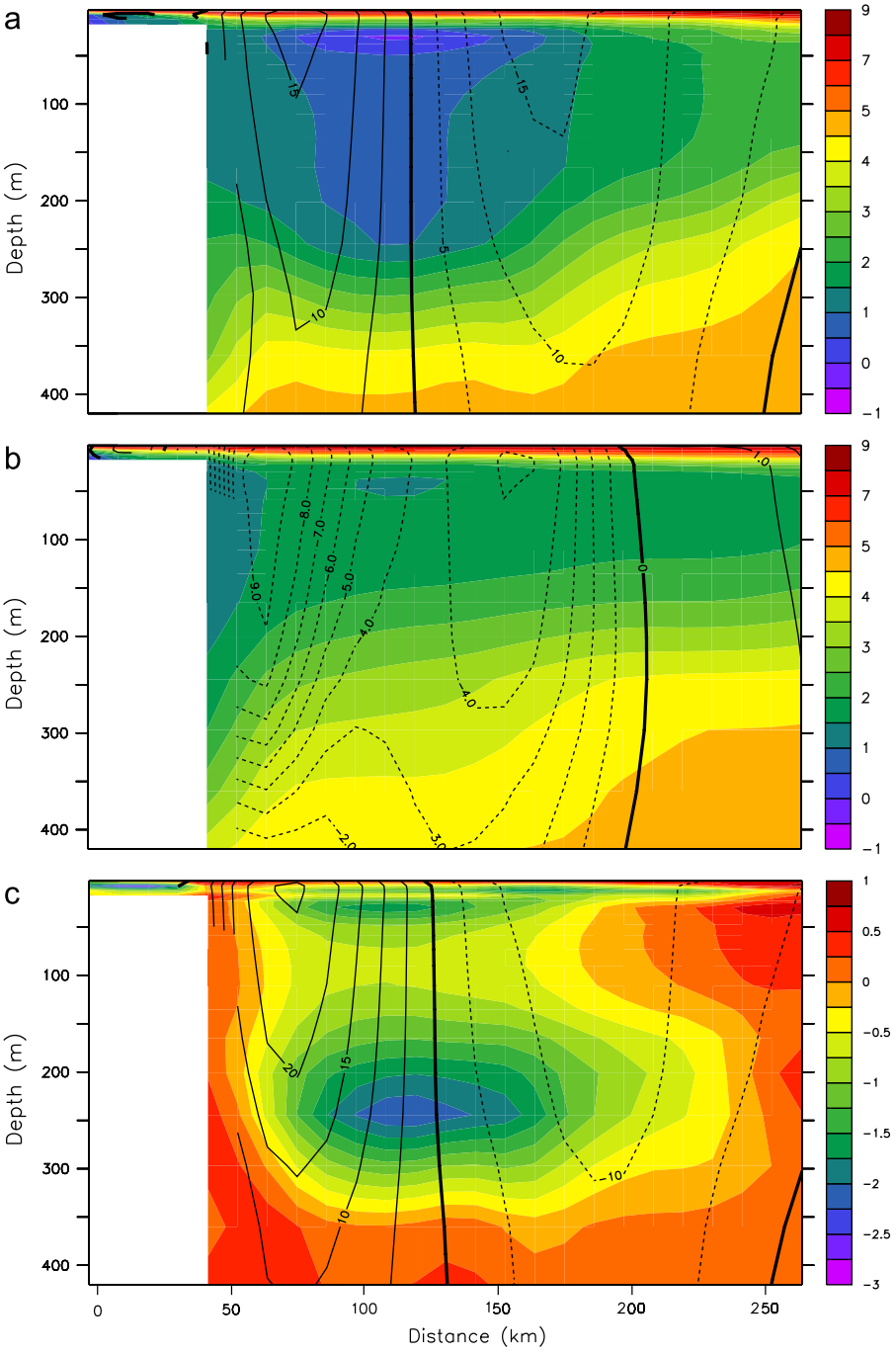


**Fig. 9.** Vertical cross-sections of potential temperature (°C; color shading) and velocity (cm/s; contours) along the green line in Fig. 8 during (a) June 1987, (b) 26-year mean June, and (c) the difference between these time periods. Solid contour lines indicate northward velocity and dashed lines indicate southward velocity (For interpretation of the references to color in this figure legend, the reader is referred to the web version of this article.).

fresher at the surface. Rogachev and Gorin (2004) observed salinities of $<33$ psu in an eddy near Kamchatka Strait during April 1991.

Animations (not shown) of monthly mean velocity and sea surface height anomaly show that over the 26-year simulation (1979–2004), the Kamchatka Current was continuously populated with meanders and southwestward-moving anticyclonic eddies, such as the one just described. The diameters of these eddies were 83–139 km and the lifetimes were typically a few months. This is corroborated by observations of eddies with similar trajectories (Rogachev and Gorin, 2004; Rogachev and Carmack, 2002). Okkonen (1993) suggested that the anticyclonic eddies found in the western Bering Sea, such as the ones found within the path of the Kamchatka Current, may be related to planetary topographic waves.

### 5.2. Eddies in the Alaskan stream

Maslowski et al. (2008a) discussed anticyclonic eddies that propagate along the path of the Alaskan Stream with an average diameter of 168 km and phase speed of approximately 2.3 km day$^{-1}$. These are similar to observations by Okkonen (1992), as well as those of Crawford et al. (2000) who detected the presence of six anticyclonic eddies over a period of seven years with an average diameter

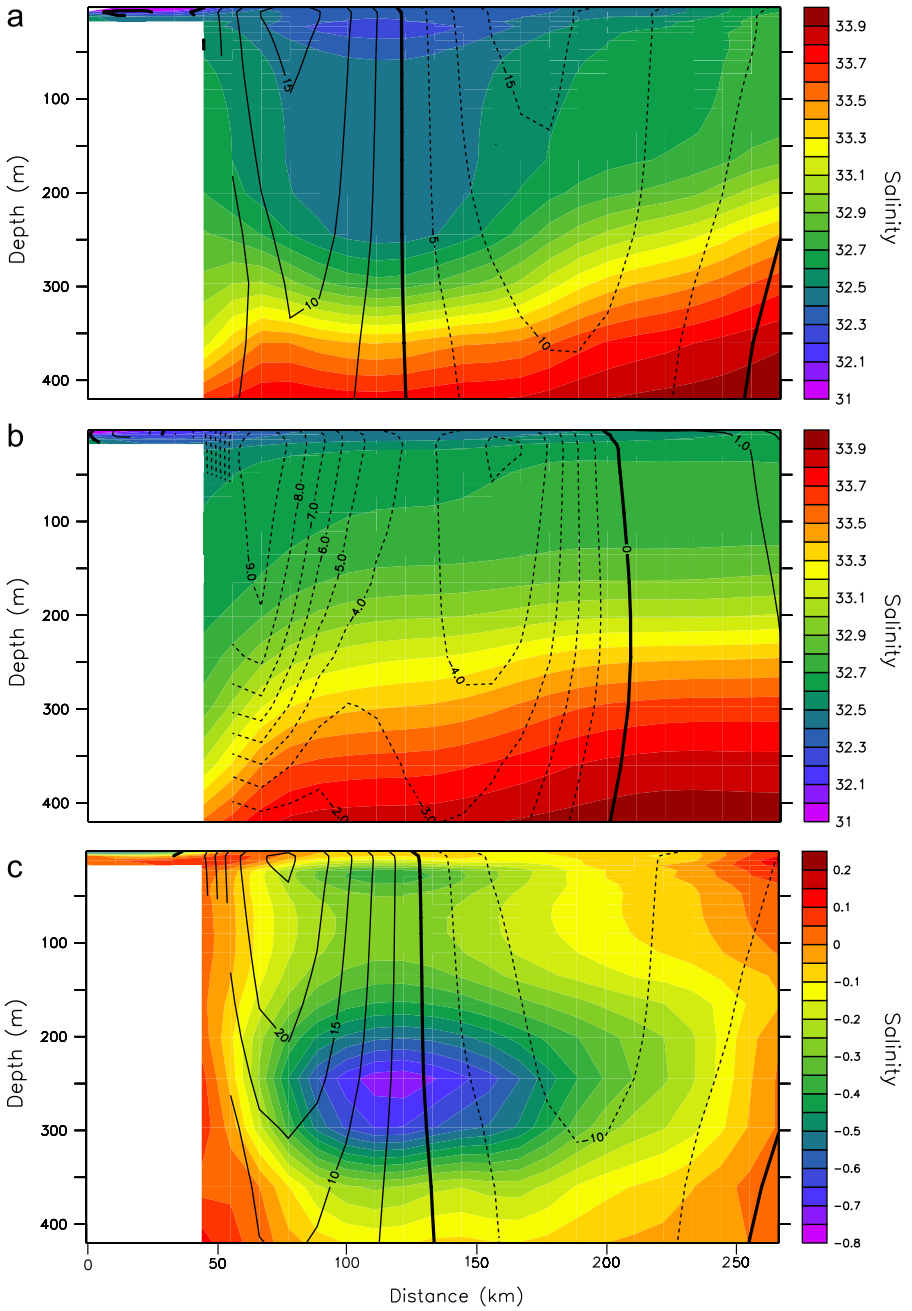


**Fig. 10.** Vertical cross-sections of salinity (color shading) and velocity (cm/s; contours) along the green line in Fig. 8 during (a) June 1987, (b) 26-year mean June, and (c) difference between these time periods. Solid contour lines indicate northward velocity and dashed lines indicate southward velocity (For interpretation of the references to color in this figure legend, the reader is referred to the web version of this article.).

of 160 km and a mean phase speed of approximately 2.5 km day$^{-1}$. In the model simulations, these eddies did not reduce the strength of the Alaskan Stream, however there was an off-shore (or southward) shift in the velocity core. The mesoscale eddies were shown to have a strong effect on the volume and property fluxes through the eastern and central Aleutian passes (Maslowski et al., 2008a). Large increases in the northward volume, heat, and salt fluxes through Amukta and Amchitka passes occurred during the presence of an eddy in the Alaskan Stream (Maslowski et al., 2008a). Okkonen (1996) estimated that an eddy observed to separate from the Alaskan Stream south of Amchitka Pass represented 21% of the mean annual transport into the Bering Sea.

Model results show that the larger and deeper passes of the western Aleutian Islands are also affected by these mesoscale features. The numerous eddies and meanders of the Bering Sea and within the Alaskan Stream play a critical role in determining the flow through the western Aleutian passes and straits. As mentioned above, there were seven flow reversals in Near Strait throughout the 26-year simulation. Eddy activity in the vicinity of the strait has a strong impact on the flow through the strait. Fig. 11 shows the local circulation in the upper 400 m during each of the seven flow reversals. There does not appear to be a consistent circulation regime associated with a flow reversal, instead the reversals occur due to the relative positions of multiple eddies and meanders both north and south of Near Strait. For example, during October 1982 (Fig. 11), mesoscale activity modified the flow through Near Strait: on the eastern side, a large anticyclone modified the path of the Alaskan Stream inflow and on the western side, anticyclonic flow is found within the strait, creating a strong southward flow. A total of 18.6 Sv flowed southward at

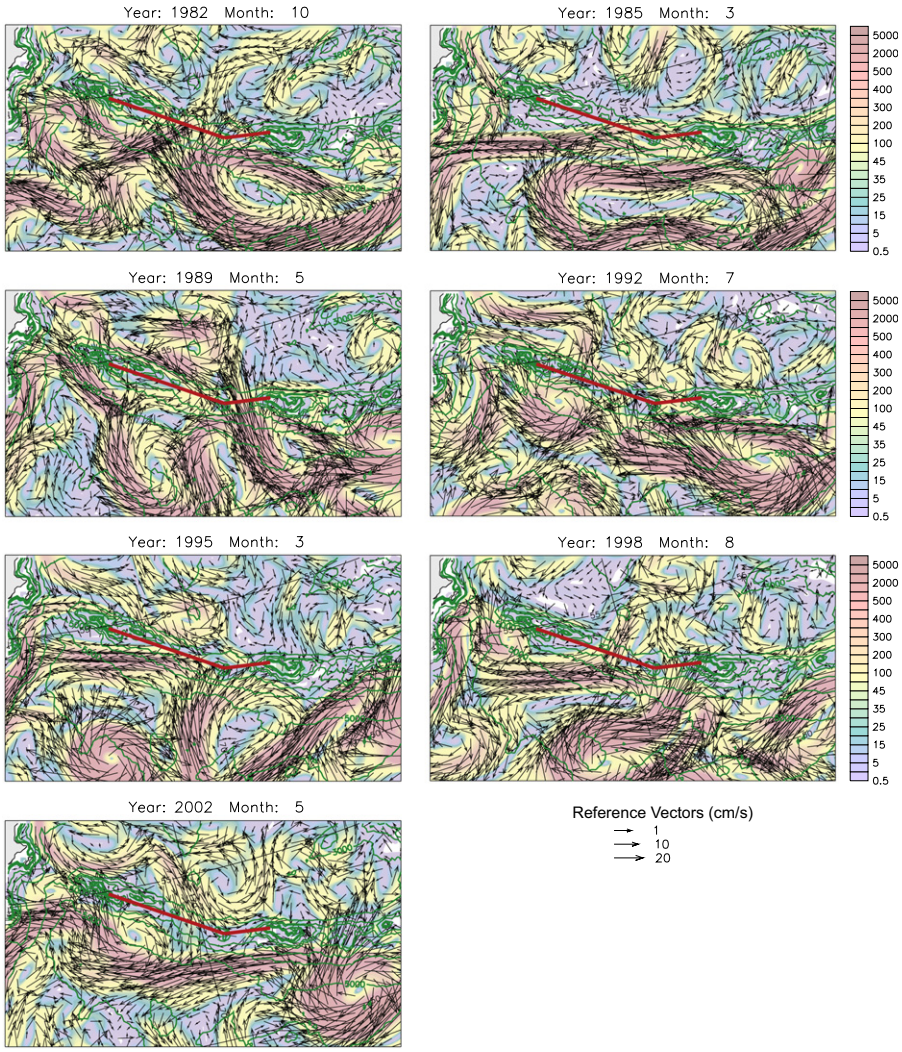


**Fig. 11.** Monthly mean total kinetic energy (shading; $cm^2/s^2$) and velocity vectors (cm/s) in the upper 400 m during each of the flow reversals as shown in Fig. 4. The year and month are indicated above each panel. The red line indicates the position of Near Strait and the green contour lines indicate bathymetry (For interpretation of the references to color in this figure legend, the reader is referred to the web version of this article.).

this time, with 11 Sv flowing northward, which equaled a net southward flux of 7.6 Sv. In March 1985, a large anticyclone has pushed part of the Alaskan Stream into Near Strait, causing a northward flow on the eastern side of the strait and a southward flow on the western side. At the same time, the anticyclone is blocking northward flow through the strait. During May 1989, an anticyclone is actually responsible for a northward flow (10.5 Sv) in the eastern part of Near Strait, however a stronger southward flow (14.3 Sv) exists across the western part of the strait (likely due to a cyclone to the north), which gives a net southward transport of 3.8 Sv. Anticyclonic blocking occurs again in July 1992, March 1995, and May 2002. August 1998 shows a strong southward flow in the central part of Near Strait, which originates in the Bering Sea, due to local cyclonicity.

Four local maxima are identified in the time series of volume transport through Near Strait (Fig. 4). Similar to the flow reversals, these maxima are predominately caused by eddies and meanders both north and south of the strait. During June 1983, the northern part of a large, irregularly shaped anticyclone reached into the strait, thereby creating a strong net northward flow (17.7 Sv; Fig. 12). Note that this same anticyclone contributed to a flow reversal 8 months earlier by blocking northward flow in the eastern part of the strait (Fig. 11). The October 1988 circulation pattern is quite complex, however a strong northward flow in the central part of the strait appears to be related to an anticyclonic meander of the Alaskan Stream. January 1994 and March 1996 both show upstream anticyclones that are pushing water northward through the eastern part of Near Strait.

## 6. Conclusions

Results presented herein are to our knowledge the first from a high-resolution, multi-decadal simulation of the entire Bering Sea, the Aleutian Island Passes and the northern North Pacific including the Gulf of Alaska and the Western Subarctic Gyre. Utilizing a large pan-Arctic domain with a non-prescribed Alaskan Stream and Aleutian throughflow allows reproduction of meanders and eddies in the Alaskan Stream and Kamchatka Current (Fig. 8) similar to those that have been observed previously (e.g. Crawford et al., 2000; Rogachev and Carmack, 2002; Rogachev and Gorin, 2004). Strong interannual variability in flow through Near Strait (Fig. 4) was simulated by the NAME model, which represents the range of variability that has been observed (Stabeno and Reed, 1992; Reed and Stabeno, 1993). Previous modeling work by Overland et al. (1994) showed a range of variability in the Near Strait inflow between approximately 5–7 Sv (see Fig. 7 in Overland et al. 1994) over a period of ten years (sampled daily), whereas NAME simulates variability between −9.5 and 18.3 Sv over

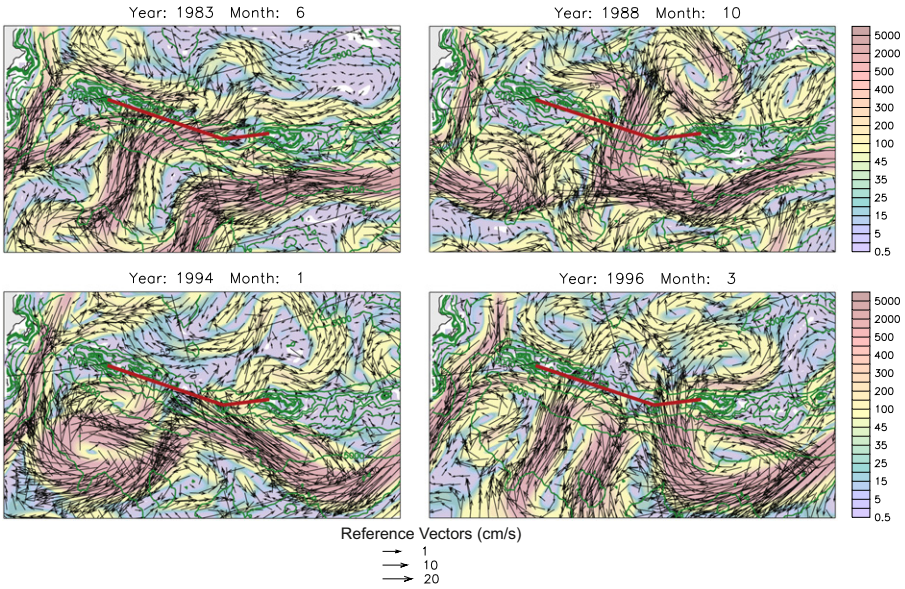


**Fig. 12.** Monthly mean total kinetic energy (shading; $cm^2/s^2$) and velocity vectors (cm/s) in the upper 400 m during each of the flow maxima as shown in Fig. 4. The year and month are indicated above each panel. The red line indicates the position of Near Strait and the green contour lines indicate bathymetry (For interpretation of the references to color in this figure legend, the reader is referred to the web version of this article.).

a period of 26 years (sampled monthly; Fig. 4). The modeled net northward flow through Near Strait approached zero and reversed 7 times from 1979–2004 for time periods of three months to two years. This was found to be related to the presence of eddies and meanders both north and south of the strait. There does not appear to be a consistent pattern responsible for inducing a reversal. Instead, reversals occur when mesoscale features are in the proper alignment with the axis of the strait. Therefore, it is believed that short-term observations (months to years) may not be representative of the actual mean flow. This indicates a need for continuous monitoring of the flow through Near Strait.

During the 26-year simulation, meanders and eddies are continuously present in the Kamchatka Current, as well as elsewhere throughout the Bering Sea. This is consistent with results from Cokelet and Stabeno (1997), which show that the background flow in the interior of the Bering Sea is dwarfed by the energetic eddies which populate the region. Our results indicate that these eddies are important in redistributing temperature and salinity, which may have an effect on biological species in the region by changing environmental conditions.

## Acknowledgments

We thank the Department of Energy Climate and Environmental Sciences Division of the Biological and Environmental Research program, National Science Foundation Office of Polar Programs, and the Office of Naval Research for support of this research. Computer resources were provided through the US Department of Defense High Performance Computer Modernization Program (HPCMP). We also thank the editor and two anonymous reviewers for insightful comments, which improved an earlier version of this manuscript.

## References

Arsen'ev, V.S., 1967. Currents and water masses of the Bering Sea, Izdatel'stro. Nauka.

Bond, N.A., Overland, J.E., Turet, P., 1994. Spatial and temporal characteristics of the wind forcing of the Bering Sea. J. Climate 7, 1119–1130.

Brooks, D.A., 1994. A model study of the buoyancy driven circulation in the Gulf of Maine. J. Phys. Oceanogr. 24, 2387–2412.

Chelton, D.B., deSzoeke, R.A., Schlax, M.G., Naggar, K.E., Siwertz, N., 1998. Geographical variability of the first baroclinic Rossby radius of deformation. J. Phys. Oceanogr. 28, 433–460.

Clement Kinney, J., Maslowski, M., 2008. Results of recent Pacific-Arctic ice-ocean modeling studies at the Naval Postgraduate School. Chin. J. Polar Sci. 19 (2), 230–236.

Clement Kinney, J., Maslowski, W., Okkonen, S., 2009. On the processes controlling shelf-basin exchange and outer shelf dynamics in the Bering Sea. Deep-Sea Res. II 56, 1351–1362, http://dx.doi.org/10.1016/j.dsr2.2008.10.023.

Crawford, W.R., Cherniawski, J.Y., Forman, M.G.G., 2000. Multi-year meanders and eddies in the Alaskan Stream as observed by TOPEX/Poseidon altimeter. Geophys. Res. Lett. 27 (7), 1025–1028.

Cokelet, E.D., Schall, M.L., Dougherty, D.M., 1996. ADCP-referenced geostrophic circulation in the Bering Sea Basin. J. Phys. Oceanogr. 26, 1113–1128.

Cokelet, E.D., Stabeno, P.J., 1997. Mooring observations of the thermal structure, density stratification and currents in the southeast Bering Sea basin. J. Geophys. Res. 102 (C10), 22947–22964.

Dukowicz, J.K., Smith, R.D., 1994. Implicit free-surface method for the Bryan-Cox-Semtner ocean model. J. Geophys. Res. 99, 7791–8014.

Endoh, M.C., Mooers, C.N.K., Johson, W.R., 1981. A coastal upwelling circulation model with eddy viscosity depending upon Richardson number. In: Richards, F.A. (Ed.), Coastal Upwelling, Coastal and Estuarine Sciences. American Geophysical Union, Washington, D. C.

Ezer, T., Oey, L.Y., 2010. The role of the Alaskan Stream in modulating the Bering Sea climate. J. Geophys. Res. 115, C04025, http://dx.doi.org/10.1029/2009JC005830.

Favorite, F., 1974. Flow into the Bering Sea through Aleutian Island passes. In: Hood, D.W., Kelley, E.J. (Eds.), Oceanography of the Bering Sea. University of Alaska, Fairbanks.

Favorite, F., 1976. Oceanography of the subarctic Pacific region, 1960–1971. Bull. Int. North Pacific Fish. Commission 33, 1–187.

Hu, H., Wang, J., 2010. Modeling effects of tidal and wave mixing on circulation and thermohaline structures in the Bering Sea: process studies. J. Geophys. Res 115, C01006, http://dx.doi.org/10.1029/2008JC005175.

Hughes, F.W., Coachman, L.K., Aagaard, K., 1974. Circulation, transport and water exchange in the western Bering Sea. In: Hood, D.W., Kelley, E.J. (Eds.), Oceanography of the Bering Sea. University of Alaska, Fairbanks.

Jakobsson, M., Cherkis, N., Woodward, J., Macnab, R., Coakley, B., 2000. New grid of Arctic bathymetry aids scientists and mapmakers. Eos Trans. Am. Geophys. Union 81 (9), 89.

Killworth, P.D., Stainforth, D., Webb, D.J., Patterson, S.M., 1991. The development of a free surface Bryann-Cox-Semtner ocean model. J. Phys. Oceanogr. 21, 1333–1348.

Kinder, T.H., Schumacher, J.D., Hansen, D.V., 1980. Observations of a baroclinic eddy: an example of mesoscale variability in the Bering Sea. J. Phys. Oceanogr. 10, 1228–1245.

Maslowski, W., Marble, D., Walczowski, W., Schauer, U., Clement, J.L., Semtner, A.J., 2004. On climatological mass, heat, and salt transports through the Barents Sea and Fram Strait from a pan-Arctic coupled ice-ocean model simulation. J. Geophys. Res. 109 (C03032)http://dx.doi.org/10.1029/2001JC001039.

Maslowski, W., Roman, R., Clement Kinney, J., 2008a. Effects of mesoscale eddies on the flow of the Alaskan Stream. J. Geophys. Res. 113, C07036, http://dx.doi.org/10.1029/2007JC004341.
Maslowski, W., Clement Kinney, J., Marble, D.C., Jakacki, J., 2008b. Towards eddy-resolving models of the Arctic Ocean. In: Hecht, M.W., Hasumi, H. (Eds.), Ocean Modeling in an Eddying Regime, Geophysical Monograph Series, Volume 177. American Geophysical Union, Washington, DC.
Mesinger, F., Arakawa, A., 1976. Numerical methods used in atmospheric models. WMO-ICSU Joint Organizing Committee, 64.
Munk, W.H., Anderson, E.R., 1948. Notes on a theory of a thermocline. J. Mar. Res. 7, 276–295.
Okkonen, S.R., 1992. The shedding of an anticyclonic eddy from the Alaskan Stream as observed by the GEOSAT altimeter. Geophys. Res. Lett. 19 (24), 2397–2400.
Okkonen, S., 1993. Observations of topographic planetary waves in the Bering slope current using geosat altimeter. J. Geophys. Res. 98 (12), 22,603–22,613.
Okkonen, S.R., 1996. The influence of an Alaskan Stream eddy on flow through Amchitka Pass. J. Geophys. Res. 101 (C4), 8839–8851.
Ohtani, K., 1970. Relative transport in the Alaskan Stream in winter. J. Oceanogr. Soc. Jpn 26, 271–282.
Overland, J.E., Spillane, M.C., Hurlburt, H.E., Wallcraft, A.J., 1994. A numerical study of the circulation of the Bering Sea basin and exchange with the North Pacific Ocean. J. Phys. Oceanogr. 24, 736–758.
Paluszkiewicz, T., Niebauer, H.J., 1984. Satellite observations of circulation in the eastern Bering Sea. J. Geophys. Res. 89, 3663–3678.
Panteleev, G.G., Stabeno, P., Luchin, V.A., Nechaev, D.A., Ikeda, M., 2006. Summer transport estimates of the Kamchatka current derived as a variational inverse of hydrophysical and surface drifter data. Geophys. Res. Lett. 33, L09609, http://dx.doi.org/10.1029/2005GL024974.
Panteleev, G., Yaremchuk, M., Stabeno, P.J., Luchin, V., Nechaev, D.A., Kikuchi, T., 2011. Dynamic topography of the Bering Sea. J. Geophys. Res. 116, C05017, http://dx.doi.org/10.1029/2010JC006354.
Reed, R.K., 1984. Flow of the Alaskan Stream and its variations. Deep-Sea Res. 31, 369–386.
Reed, R.K., Stabeno, P.J., 1993. The recent return of the Alaskan Stream to near strait. J. Mar. Res. 51, 515–527.
Rogachev, K., Carmack, E., 2002. Evidence of trapping and amplification of near-inertial motions in a large anticyclonic ring in the Oyashio. J. Oceanogr. 58, 673–682.
Rogachev, K.A., Gorin, I.I., 2004. Mass transport and long-term evolution of eddies in the Kamchatka current. Oceanology 44 (1), 15–21.
Rogachev, K., Shlyk, N., Carmack, E., 2007. The shedding of mesoscale anticyclonic eddies from the Alaskan Stream and westward transport of warm water. Deep-Sea Res. II 54, 2643–2656.
Royer, T.C., 1981. Baroclinic transport in the Gulf of Alaska, part II. A freshwater driven coast current. Journal of Marine Research 39, 251–266.
Salmon, D.K. (1992) On interannual variability and climate change in the North Pacific. Dissertation, University of Alaska, Fairbanks.
Schumacher, J.D., Stabeno, P.J., 1994. Ubiquitous eddies of the eastern Bering Sea and their coincidence with concentrations of larval pollock. Fish. Oceanogr. 3, 182–190.
Semtner, A.J., 1995. Modeling ocean circulation. Science 269, 1379–1385.
Semtner, A.J., Chervin, R.M., 1992. Ocean circulation from a global eddy-resolving model. J. Geophys. Res. 97, 5493–5550.
Solomon, H., Ahlnäs, K., 1978. Eddies in the Kamchatka Current. Deep-Sea Res. 25, 403–410.
Springer, A.M., Piatt, J.F., Shuntov, V.P., Van Vliet, G.B., Vladimirov, V.L., Kuzin, A.E., Perlov, A.S., 1999. Marine birds and mammals of the Pacific Subarctic Gyres. Prog. Oceanogr. 43, 443–487.
Stabeno, P.J., Reed, R.K., 1992. A major circulation anomaly in the western Bering Sea. Geophys. Res. Lett. 19, 1671–1674.
Stabeno, P.J., Reed, R.K., 1994. Circulation in the Bering Sea Basin observed by satellite-tracked drifters: 1986–1993. J. Phys. Oceanogr. 24, 848–854.
Stabeno, P.J., Schumacher, J.D., Ohtani, K., 1999. The physical oceanography of the Bering Sea. In: Loughlin, T.R., Ohtani, K. (Eds.), Dynamics of the Bering Sea. University of Alaska Sea Grant, Fairbanks, AK.
Stabeno, P.J., Ladd, C., Reed, R.K., 2009. Observations of the Aleutian North Slope Current, Bering Sea, 1996–2001. J. Geophys. Res. 114, C05015, http://dx.doi.org/10.1029/2007JC004705.
Steele, M., Morley, R., Ermold, W., 2001. PHC: a global ocean hydrography with a high quality Arctic Ocean. J. Climate 14 (9), 2079–2087.
Verkhunov, A.V., Tkachenko, Y.Y., 1992. Recent observations of variability in the western Bering Sea current system. J. Geophys. Res. 97, 14,369–14,376.
Wang, J., Hu, H., Mizobata, K., Saitoh, S., 2009. Seasonal variations of sea ice and ocean circulation in the Bering Sea: a model-data fusion study. J. Geophys. Res. 114, C02011, http://dx.doi.org/10.1029/2008JC004727.
Zhang, J.Z., Woodgate, R., Moritz, R., 2010. Sea ice response to atmospheric and oceanic forcing in the Bering Sea. J. Phys. Oceanogr. 40, 1729–1747.